CHEMISTRY OF MATERIALS

Article

pubs.acs.org/cm

Storage of Visible Light for Long-Lasting Phosphorescence in Chromium-Doped Zinc Gallate

Aurélie Bessière,*[,†] Suchinder K. Sharma,[†] Neelima Basavaraju,[‡] Kaustubh R. Priolkar,[‡] Laurent Binet,[†] Bruno Viana,[†] Adrie J. J. Bos,[§] Thomas Maldiney,[⊥,#] Cyrille Richard,[⊥,#] Daniel Scherman,[⊥,#] and Didier Gourier*[,†]

[†]Institut de Recherche de Chimie Paris, CNRS − Chimie ParisTech, 11 rue Pierre et Marie Curie, 75005 Paris, France

[‡]Department of Physics, Goa University, Goa 403206, India

[⊥]Unité de Pharmacologie Chimique et Génétique et d'Imagerie; UMR 8151 CNRS; U 1022 Inserm; Université Paris Descartes, Sorbonne Paris Cité, Faculté des Sciences Pharmaceutiques et Biologiques, F-75270 Paris cedex, France

[#]Chimie-ParisTech, F-75231 Paris cedex, France

[§]Faculty of Applied Sciences, Delft University of Technology, Delft, The Netherlands

Supporting Information

ABSTRACT: $ZnGa_2O_4:Cr^{3+}$ presents near-infrared long-lasting phosphorescence (LLP) suitable for in vivo bioimaging. It is a bright LLP material showing a main thermally stimulated luminescence (TSL) peak around 318 K. The TSL peak can be excited virtually by all visible wavelengths from 1.8 eV (680 nm) via d−d excitation of Cr^{3+} to above $ZnGa_2O_4$ band gap (4.5 eV−275 nm). The mechanism of LLP induced by visible light excitation is entirely localized around Cr_{N2} ion that is a Cr^{3+} ion with an antisite defect as first cationic neighbor. The charging process involves trapping of an electron−hole pair at antisite defects of opposite charges, one of them being first cationic neighbor to Cr_{N2}. We propose that the driving force for charge separation in the excited states of chromium is the local electric field created by the neighboring pair of antisite defects. The cluster of defects formed by Cr_{N2} ion and the complementary antisite defects is therefore able to store visible light. This unique property enables repeated excitation of LLP through living tissues in $ZnGa_2O_4:Cr^{3+}$ biomarkers used for in vivo imaging. Upon excitation of $ZnGa_2O_4:Cr^{3+}$ above 3.1 eV, LLP efficiency is amplified by band-assistance because of the position of $Cr^{3+4}T_1$ (^4F) state inside $ZnGa_2O_4$ conduction band. Additional TSL peaks emitted by all types of Cr^{3+} including defect-free Cr_R then appear at low temperature, showing that shallower trapping at defects located far away from Cr^{3+} occurs through band excitation.

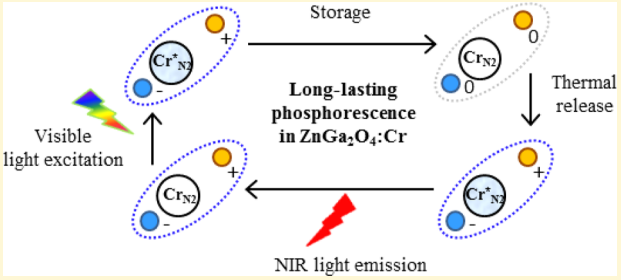

KEYWORDS: *long-lasting phosphorescence, afterglow, persistent luminescence, spinel, $ZnGa_2O_4$, Cr^{3+}, thermally stimulated luminescence, storage, near-infrared*

INTRODUCTION

Persistent luminescence of materials, also known as long-lasting phosphorescence (LLP), is based on the transient storage of radiation in the form of trapped electrons and holes, followed by the slow detrapping and radiative recombination of the carriers. This gives rise to a visible-light emission lasting for minutes or hours, suitable for many applications as night or dark environment vision displays (emergency signs, toys, etc.).[1] When light emission occurs in the region of partial transparency of living tissues, that is, in the far red to near-infrared, LLP nanoparticles can be used for in vivo imaging of small animals[2,3] as well as active targeting of various cancerous cells in vitro through specific ligand/receptor interaction.[4,5] As a major asset of the technique, the particles can be excited ex vivo before injection, which circumvents autofluorescence otherwise observed when living tissues are also excited. Classical mechanism of LLP, and more generally of thermally stimulated luminescence (TSL), is based on the generation of free electrons and holes by UV, X-ray, or γ-ray irradiation, namely with a radiation energy that is larger than the band gap energy of the compound.[6] Free carriers then get trapped by lattice defects, impurities, or codopants in the material. Light emission occurs by thermally assisted release of the carriers and recombination at luminescent centers, such as transition metal ions,[7] or much more generally lanthanide cations.[8−10] LLP is a special case of TSL, wherein the trap depth is of the order of 0.5 to 1 eV, allowing a progressive thermal release of carriers at room temperature (RT) and therefore a continuous

Received: September 12, 2013
Revised: November 27, 2013
Published: November 27, 2013

radiative recombination and emission of light. LLP for in vivo imaging can be optimized by controlling the emitting center (wavelength of the emission) and the nature of the trapping defects (intensity and duration of the persistent luminescence).[11−13]

Zinc gallate $ZnGa_2O_4$ (ZGO) is an AB_2O_4 compound with spinel structure and Zn^{2+} and Ga^{3+} ions occupying tetrahedral A and octahedral B sites, respectively (Figure 1). Although it is most widely considered as a normal spinel, it exhibits a slight inversion character,[14,15] wherein a few percent of Zn^{2+} and Ga^{3+} occupy B and A sites, respectively. Such defects in the host matrix are called antisite defects and are just a Zn ion at a Ga site and a Ga ion at a Zn site (noted Zn'_{Ga} and Gn°_{Zn} in Kröger−Vink notation, respectively) in an ideal normal spinel structure type. ZGO exhibits about 3% inversion, which means that ∼3% of Zn^{2+} occupy Ga sites, and correlatively the same amount of Ga^{3+} occupy Zn sites.[15] When doped with Cr^{3+} ions, ZGO becomes a high brightness LLP material with an emission spectrum perfectly matching the transparency window of living tissues.[16] It allows in vivo mouse imaging with a high signal to background ratio.[17] $ZnGa_2O_4$:Cr^{3+} (ZGO:Cr) constitutes a second-generation LLP probe with enhanced properties for bioimaging relative to the first generation phosphate[18,19] or silicate[11] materials designed for LLP imaging and excited only with X-ray or UV radiation. The most interesting characteristic of ZGO:Cr lies in the fact that its LLP can be excited with orange-red light, well below its band gap energy and in the transparency window of living tissues.[17] Repetitive in vivo excitation with orange-red light is therefore possible to trigger again and again the LLP of injected particles. Thanks to this distinctive property, ZGO:Cr nanoparticles could be observed for tens of hours in living mice and allowed to assess the slow accumulation of stealth ZGO:Cr nanoparticles in tumors.[17]

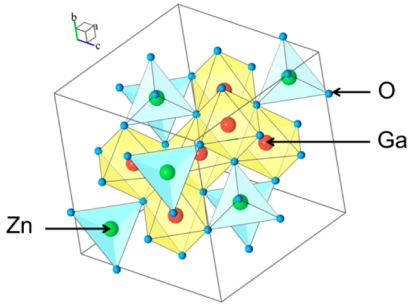

Figure 1. Cubic spinel structure of ZGO.

After the first report on LLP emitted by ZGO:Cr in the near-infrared[16] and its use for in vivo imaging,[17] the interest in the Cr-doped spinel family has recently further increased. Pan et al[20] and Allix et al[15] reported an enhanced LLP efficiency for germanium substituted $ZnGa_2O_4$:Cr, in possible relation to the amount of antisite defects. Zhuang et al showed that ZGO:Cr could also be improved by Bi codoping.[21] An intriguing question therefore arises about the origin of such a bright persistent luminescence in this family of materials. In this paper, we investigated the role of the antisite defects both in the neighborhood of and far away from Cr^{3+} doping ions in the TSL process over a wide temperature range (10−600 K). The cubic spinel structure is presented in Figure 1. By considering Cr^{3+} occupying gallium site, for example, the central position in Figure 1, we find that statistical defects may occur at various distances: zinc in the gallium site (Zn_{Ga}) at short distances (0.295 nm) and gallium in the zinc site (Ga_{Zn}) at longer distances (0.346 and 0.541 nm). We show that the charging step of the LLP does not involve any valence state modification of Cr^{3+} during excitation/storage steps, indicating that both electron and hole are trapped at other lattice defects. For excitation above ∼3.1 eV, electron and hole migrate via host bands, and traps distributed all over the material are filled during storage. For excitation below ∼3.1 eV, including excitation by orange-red light, trapping defects are localized in the close vicinity of Cr^{3+} ions. The mechanism proposed here implies that visible light is stored as excited metastable states of specific clusters formed by Cr^{3+} doping ion and a pair of neighboring antisite defects.

EXPERIMENTAL METHODS

Materials preparation. ZGO:Cr powder was synthesized by the solid-state method. Appropriate quantities of ZnO (Sigma Aldrich 99.99% pure), Ga_2O_3 (Sigma Aldrich 99.99% pure), and CrO_3 (SRL 99% pure) were mixed and carefully ground in an agate mortar with propan-2-ol. A pellet was prepared from the powder mixture and fired in air at 1300 °C. The compound was prepared with a Cr content of 0.5 at % relative to Ga. A nominal 1% Zn deficiency relative to stoichiometry was introduced in the reactants ratio (Zn/(Ga+Cr) = 0.495) as this was shown to improve LLP of ZGO:Cr powders prepared by the solid-state route.[16] However, it is stressed that the 1% Zn deficiency is only at the initial sample preparation stage. ZnO and Ga_2O_3 partially evaporate during high-temperature annealing. In our samples, an initial ∼1% Zn deficiency gives the best crystalline order in the final material compared to samples synthesized with stoichiometric starting compounds, when monitored through optical and electron paramagnetic resonance (EPR) spectroscopy techniques (not reported in this article). EPR lines are very narrow in this case, pointing to a minimal strain broadening. We infer that this small Zn deficiency provides best compensation for the parallel evaporation of ZnO and Ga_2O_3, achieving the longest range order. X-ray diffraction assessed a $Fd\bar{3}m(O_h^7)$ cubic phase free from any impurity.

Characterization Methods. Photoluminescence (PL) measurements were performed at RT using a Varian Cary Eclipse spectrofluorimeter with a Xenon lamp as excitation source.

LLP measurements were carried out on 0.2 g of powder samples stacked into 1 cm-diameter sample-holder. The sample was first excited for 15 min with a monochromatic excitation provided by the third harmonic of a YAG:Nd pulsed laser pumped by an optical parametric oscillator (OPO). Its luminescence was detected via an optical fiber using a Scientific Pixis 100 CCD camera cooled at −65 °C coupled with an Acton SpectraPro 2150i spectrophotometer for spectral analysis.

TSL measurements were performed with two different setups. In the first one, a fiber-coupled grating monochromator in combination with a Xenon arc lamp allowed the monochromatic excitation of the sample at RT. A Risø-Thermoluminescence reader (TL/OSL-DA-15) collected TSL glow curves via a red light sensitive photomultiplier tube with an optical filter (LOT-ORIEL 700FS380) in front of it at a heating rate of 5 K/s. The setup was fully automated and software controlled to allow successive recording of multiple glow curves and construction of TSL excitation spectrum. Fifty TSL glow curves were recorded successively at RT with excitation wavelength varying from 200 to 710 nm, every 10 nm, starting with a 10 s excitation period of the sample.[22] In the second setup, the sample prepared as a thin pressed pellet and silver glued on the coldfinger of a cryostat was excited at 10 K across the cryostat quartz window. The excitation was carried out with monochromatic excitation produced by the third harmonic of a YAG:Nd pulsed laser pumped by an OPO. TSL was detected via an optical fiber using a Scientific Pixis 100 CCD camera cooled at −65 °C coupled with an Acton SpectraPro 2150i spectrometer for spectral analysis while a heating rate of 10 K/min was applied. TSL glow curves were drawn by plotting the integrated luminescence intensity over 640−760 nm.

Transmission measurements were performed with a Varian Cary UV−vis-NIR-spectrophotometer 6000i model. The powder sample was mixed with KBr powder in a 9:1 ratio and an 1 cm diameter pellet was prepared. A separate pellet of pure KBr was used for baseline correction. The two pellets were placed into a cryostat equipped with two transparent windows.

Continuous wave EPR spectra were recorded at 10K on a Bruker ELEXSYS E500 spectrometer working at X-band (9.445 GHz). The microwave power was 0.2 mW and the modulation depth was 1 mT at 100 kHz. During EPR experiment, the sample was excited in situ in the EPR cavity with the infrared filtered radiation of a UV lamp (200−900 nm) from Ushio UXL306−500 W.

RESULTS AND DISCUSSION

In a $ZnGa_2O_4$ host, Cr^{3+} ion readily substitutes Ga^{3+} in its slightly trigonally distorted octahedral site.[23] The first evidence of the central role of one special type of Cr^{3+} ions in the LLP process is highlighted by the comparison of PL and LLP spectra. Three PL spectra of ZGO: Cr recorded at RT are shown in Figure 2a for different excitation wavelength.

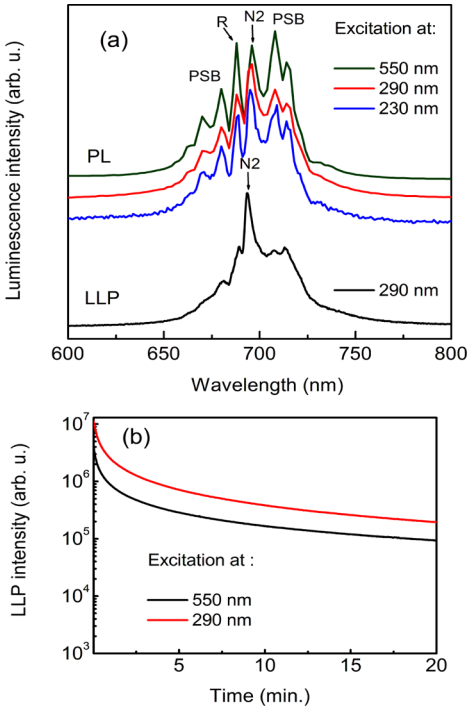

Figure 2. (a) Normalized PL spectra of ZGO:Cr and LLP emission spectrum at RT, 10 s after the end of a 290 nm excitation; (b) LLP decays measured after a 15 min laser excitation at 550 nm (11 mJ) and 290 nm (3 mJ).

They show the ^2E (^2G) → $^4A_2$ (^4F) transition of Cr^{3+} (d^3 ion) in an octahedral crystal field. The zero phonon R lines, observed at 688 nm, correspond to Cr^{3+} in unperturbed octahedral sites, whereas an N2 line, at 695 nm, is ascribed to Cr^{3+} ions with a neighboring antisite defect.[24−26] The two expected components of the R line, R1 and R2, cannot be distinguished at RT because of poor instrument resolution. The R lines are accompanied by their Stokes (S) and anti-Stokes (AS) phonon side bands (PSB) peaking at 708 and 715 nm on the one hand (S) and 663, 670, and 680 nm on the other (AS). PSB of N2 lines also exist in the 650−750 nm range but present broader and less intense features than PSB of R lines.[27] The corresponding PL excitation spectrum of Cr^{3+} emission is shown in Figure 3 as black line. The O^{2-} (2p) to Ga^{3+}, Zn^{2+} (4s, 4p) charge transfer band responsible for band gap

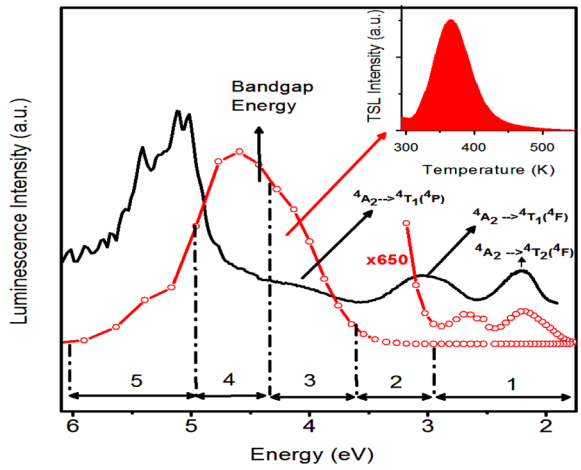

Figure 3. PL excitation spectrum recording emission at 695 nm (black line) compared to TSL excitation spectrum (red open circles). Insert: TSL glow curve of ZGO:Cr after 10 s excitation at RT with 300 nm wavelength of Xenon lamp.

absorption of $ZnGa_2O_4$ is observed at around 4,5 eV.[28,29] Three d−d absorption bands of Cr^{3+} are observed at 2.23 eV ($^4A_2$ (^4F) → $^4T_2$ (^4F)), 2.95 eV ($^4A_2$ (^4F) → $^4T_1$ (^4F)), and around 4.77 eV ($^4A_2$ (^4F) → $^4T_1$ (^4P)), as expected from a Tanabe Sugano diagram for a d^3 ion in an octahedral crystal field.[30] It is difficult to distinguish between $Cr^{3+}$$^4A_2$ (^4F) → $^4T_1$ (^4P) band and 4.5 eV charge transfer band, as they overlap with each other.

All these bands are not single bands and double humps can be distinguished, particularly in the $^4A_2$ (^4F) → $^4T_2$ (^4F) and $^4A_2$ (^4F) → $^4T_1$ (^4F) transitions. This is mainly due to the trigonal distortion present at Ga^{3+} site, but also to the superimposition of the excitation spectra from several types of Cr^{3+} ions, among which are Cr_R and Cr_{N2}, responsible for the R and N2 zero phonon lines, respectively. It is not easy to measure distinct excitation spectra for Cr_R and Cr_{N2} emission because the difference in crystal field is small and energy transfer occurs in a large extent between the two types of chromium ions. The reader is referred to Derkosch et al.[24] where at 75 K, the $^4A_2$ (^4F) → $^4T_2$ (^4F) excitation band for the N2 emission was shown to widen by 20 nm at the long wavelength side relative to the excitation of the R emission. Here, in Figure 2, the most noticeable difference in the N2/R emission ratio is observed at RT when exciting in the $^4A_2$ (^4F) → $^4T_1$ (^4P) transition on the one hand (excitation at 230 or 290 nm), and in the $^4A_2$ (^4F) → $^4T_2$ (^4F) band on the other hand (excitation at 550 nm). The N2/R ratio is clearly higher for 230 or 290 nm excitation ($^4A_2$ (^4F) → $^4T_1$ (^4P)) than for 550 nm ($^4A_2$ (^4F) → $^4T_2$ (^4F)). This can be explained by different selection rules for the two types of Cr^{3+} ions for ^4F → ^4P and ^4F → ^4F transitions. ^4F → ^4P appears more favorable to N2 than ^4F → ^4F. The ^4F → ^4F transition (one-electron transition) is normally stronger than a ^4F → ^4P transition (two-electron transition). However the distortion of Cr_{N2} site increases the mixing of opposite parity orbitals, therefore relaxing the selection rules and leading to a more intense N2 emission in comparison to R. As a consequence, the ratio of excited Cr_{N2} over Cr_R ions is more important when the sample

dx.doi.org/10.1021/cm403050q | Chem. Mater. 2014, 26, 1365−1373

is excited at wavelengths shorter than 340 nm (340 nm is the border wavelength between $^4F \rightarrow {}^4F$ and $^4F \rightarrow {}^4P$ transitions in PL spectrum of Figure 3) than in the visible range. Figure 2a also shows the LLP emission spectrum obtained a few seconds after the end of a 15 min excitation at 290 nm. As was previously shown in TSL spectra obtained after X-ray excitation,[16] the LLP emission spectrum after UV excitation is also largely dominated by the emission from Cr_{N2} showing that this type of Cr^{3+} ion plays a specific role in the LLP process.

Persistent luminescence in ZGO:Cr is of high interest for in vivo optical imaging. Excitation of ZGO:Cr in the form of nanoparticles with UV light before their injection to a small animal triggers a LLP signal observable across the animal tissues for a couple of hours[17] (similarly to the LLP decay after 290 nm excitation shown in Figure 2b). Furthermore, a subsequent excitation with red light across the animal tissues after their injection enables the excitation of the LLP decay (similarly to the LLP decay after 550 nm excitation shown in Figure 2b). The LLP of the probes inside the animal can therefore be excited many times over a very long period (several days). This is an essential property of the material that enables to follow in vivo, the slow accumulation of LLP nanoparticles in tumors.[17]

This persistent luminescence is best investigated by TSL. A TSL glow curve of ZGO:Cr was recorded with the first setup described in the experimental part, after the sample had been illuminated at RT with the 300 nm wavelength (4.13 eV) of a Xenon lamp, corresponding to the $^4A_2 \rightarrow T_1(^4P)$ transition of Cr^{3+}. As shown in the insert of Figure 3, it is composed of a broad peak with a maximum at 365 K, responsible for the LLP phenomenon observed at RT. In order to identify the absorption bands giving rise to LLP, a series of 50 similar glow curves were successively recorded by varying the monochromatic excitation wavelength every 10 nm from 200 to 710 nm. The total area of each glow curve was reported as the TSL excitation intensity in Figure 3 (red open circles). PL and TSL excitation spectra are drawn in the same figure for comparison. The TSL excitation spectrum can be divided into five wavelength ranges indicated in the bottom of Figure 3. Over range 1, the $^4A_2 \rightarrow {}^4T_2$ (^4F) and the $^4A_2 \rightarrow {}^4T_1$ (^4F) transitions of Cr^{3+} are observed. Range 2 still corresponds to the $^4A_2 \rightarrow {}^4T_1$ (^4F) transition of Cr^{3+} but the TSL intensity starts to rise steeply in this range. Finally ranges 3 to 5 present much stronger TSL and are separated by inflection points observed on both TSL and PL excitation spectra. Range 3 belongs to the $^4A_2 \rightarrow {}^4T_1$ (^4P) transition of Cr^{3+}. Range 4 may correspond to $O^{2-} \rightarrow Ga^{3+}$,$Zn^{2+}$ excitation (band-to-band transition) as it is exactly overlapping with the ZGO bandgap and the TSL output is maximum in this region exhibiting traditional TSL mechanism. Range 5 corresponds to excitation to energy greater than the bandgap energy and is better observed in PL. As such transitions occur for Cr^{3+} complexes in solution, for example $[Cr(H_2O)_6]^{3+}$, it is likely due to ligand-to-metal charge transfer transitions (LMCT). This excitation spectrum of the 365K TSL peak shows that LLP can not only be triggered in the Cr^{3+} UV absorption band of ZGO: Cr, but also in both its visible absorption bands above 400 nm. In this case, the resulting TSL signal after visible excitation is rather weak when compared to the one recorded following UV excitation and therefore requires a significant magnification (650×) of the corresponding spectrum in order to be clearly distinguished.

A specific role of Cr_{N2} was already pointed out in Figure 2: Cr_{N2} is the main LLP emitter, i.e., the final center of the LLP mechanism. The role of Cr_{N2} in the charging step of the process, i.e., when charges are separated and trapped, can be evidenced by considering the TSL excitation spectrum of Figure 3. The red shift of the d-d excitation bands for TSL relative to the excitation bands for PL demonstrates that LLP is more efficiently triggered by the direct excitation of Cr_{N2} than by nondistinct excitation of all Cr^{3+} ions.

The steep rise of TSL intensity in range 2, corresponding to the short wavelength part of the $^4A_2 \rightarrow {}^4T_1$ (^4F) transition, is explained by the assistance of ZGO band states in the production and trapping of carriers. This is accounted for by setting the $^4T_1$ (^4F) excited state of Cr^{3+} partly degenerated with band states (that is an electron in the bottom of the CB and a hole in the top of the VB) as shown in Figure 4. The

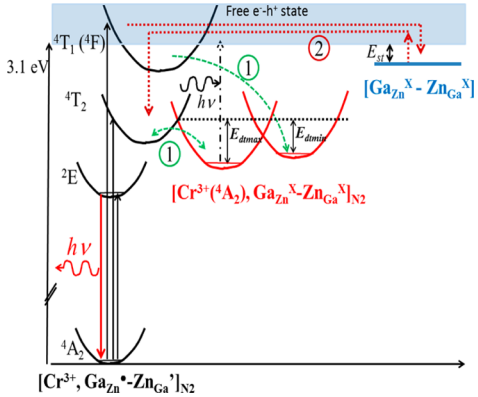

Figure 4. Energy level diagram of Cr_{N2} ion in ZGO:Cr, in a configuration coordinate representation. The blue area corresponds to host band excitation (free e^-—h^+ states). Black potentials represent Cr^{3+} states. Red potentials represent Cr_{N2} centers, i.e., Cr^{3+} with electron–hole pairs trapped at neighboring antisite defects. The blue level represents pairs of antisite defects at long distances from Cr^{3+} ion. Excitations are represented by vertical black arrows. Electron–hole trapping and release are represented by dotted green arrows when exciting below 3.1 eV (path 1) and by red dotted arrows when exciting above 3.1 eV (path 2). The interrupted black arrows represent an indirect excitation from filled deep traps.

position of all Cr^{3+} energy levels is deduced from the position of $^4T_1$ (^4F) (black curves in Figure 4). The figure shows $^4A_2$, ^2E, $^4T_2$ energy levels (range 1) and $^4T_1$ energy level (ranges 1 and 2) of Cr_{N2} in a configuration coordinate diagram. The ground state of Cr^{3+} can thus be located ~3.1 eV below the band states where charges are delocalized. The Cr^{3+} states reached when exciting at higher energy (above 3.1 eV, below 400 nm), i.e., in ranges 3, 4, and 5, are then fully degenerated with free electron–hole states and band assistance controls TSL/LLP in this case. This induces an increased probability for charge separation and carriers trapping and therefore a very intense TSL signal. Finally, band-to-band excitation (range 4) is almost as efficient as band-assisted Cr^{3+} excitations. This is again consistent with Cr^{3+} ions as the main actors in both the excitation and the emission steps of the LLP process.

The mechanism of TSL/LLP was studied in more detail with the second TSL setup. Figure 5a shows a TSL glow curve of ZGO:Cr excited at 10 K with 290 nm light (range 3 in Figure 3). It shows a main peak at 318K responsible for LLP emitted at RT. This is the same glow peak as observed with the first

dx.doi.org/10.1021/cm403050q | Chem. Mater. 2014, 26, 1365–1373

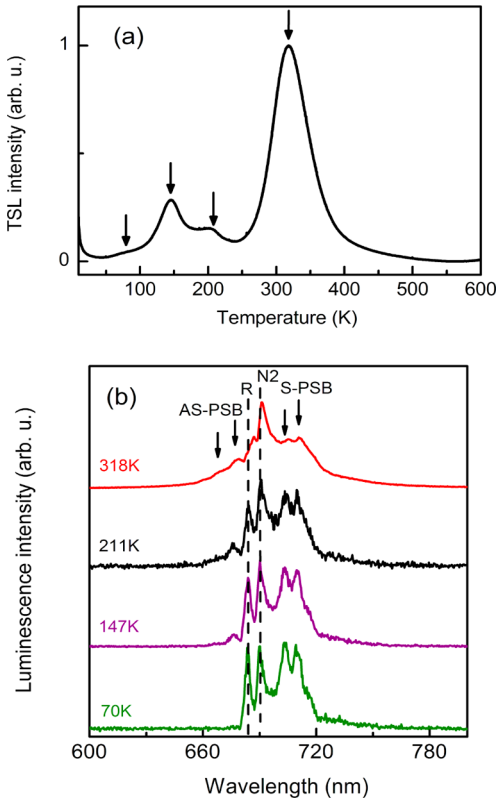

Figure 5. (a) TSL glow curve and (b) TSL spectra at varying temperatures of ZGO:Cr after 30 min excitation at 10 K with 290 nm laser.

TSL setup (inset of Figure 3), but shifted to lower temperature due to a slower heating rate. Additional low-temperature peaks are now also observed around 80, 145, and 205 K. The trap depth energies E_{st} (st = shallow traps) corresponding to the main low-temperature peaks at $T_M \approx 145$ and 205 K can be roughly estimated to be $E_{st} \approx 0.3$ and 0.4 eV, respectively, by using the expression $E_{st} \approx 25k_BT_M$.[31] The main TSL peak at $T_M \approx 320$ K has been studied in more detail using the first setup and applying two thermal cleaning methods (see the Supporting Information). The study showed that this peak is not unique and corresponds to a distribution of trap depth energies E_{dt} (dt = deep traps) in the range $E_{dt,min} \approx 0.7$ eV to $E_{dt,max} \approx 0.9$ eV.

For each point of the TSL glow curve shown in Figure 5a, the emission spectra were recorded by a CCD camera. Selected spectra at temperatures indicated by arrows in Figure 5a are gathered in Figure 5b. Cr^{3+} emission spectrum changes with temperature. As expected, AS-PSB grow with temperature. What is more interesting, the N2/R ratio of zero phonon line emissions increases with temperature. At low temperature (70 K), R lines are almost as intense as N2 and are accompanied by their intense PSB at 703 and 709 nm. As temperature increases, the contribution of N2 then becomes more and more important. In the highest temperature and main TSL peak in particular (318 K), the contribution of N2 is largely dominant. This is consistent with what was observed in Figure 2b, where the LLP spectrum was dominated by N2 line emission. Although trapping and detrapping giving rise to LLP at RT and corresponding to the TSL peak at 318 K (deep trapping) are focused on Cr_{N2}, it is interesting to observe that the release of charges from shallow traps (responsible for the low-temperature TSL peaks) induces luminescence from both Cr_R and Cr_{N2}.

Additional TSL glow curves were recorded by varying the excitation wavelength provided by a laser. The glow curves normalized to the main peak intensity are presented in Figure 6. The excitation wavelengths were selected along the TSL

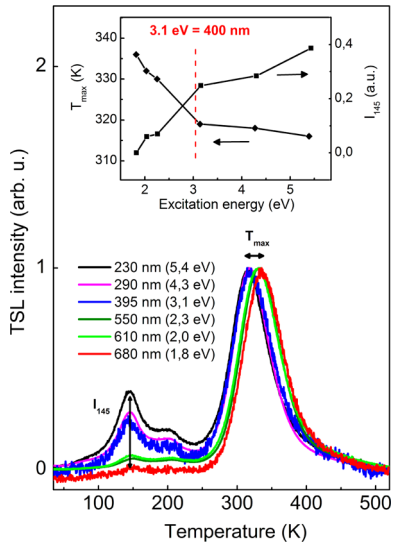

Figure 6. Normalized TSL glow curves of ZGO:Cr after 5 min excitation at 10 K with various laser wavelength excitations. Insert: Variation with the excitation energy of the TSL intensity at 145 K (T_1) and of the temperature of the main TSL peak maximum (T_{main}).

excitation range presented in Figure 3. First a TSL glow curve similar to the one shown in Figure 5a can be recorded even when the Cr^{3+} ions are excited with 680 nm (1.8 eV) visible light, corresponding to the low energy tail of the $^4A_2 \rightarrow {}^4T_2$ and the spin forbidden $^4A_2 \rightarrow {}^2E$ transitions. The TSL intensity is weak but it is still clearly observable. This gives another indication that the mechanism of charge trapping/detrapping is localized in the close vicinity of Cr^{3+} ions, as $^4T_2$ and ^2E are well below the CB edge.

With 680 nm excitation, the low-temperature TSL peaks (below 250 K) are almost not observed anymore. With $^4A_2 \rightarrow {}^4T_2$ excitation (550 and 610 nm excitations), these peaks become observable but present a weak intensity. As excitation wavelength shortens, the intensity of these low-temperature peaks grows up relative to the main peak, with a maximum relative intensity for 230 nm (5.4 eV) excitation. Moreover, varying the excitation wavelength induces a shift in the position of the main peak maximum. The inset of Figure 6 shows on the one hand the variation in the peak intensity at 145 K (noted I_{145}) as a function of the excitation energy (right scale) and on the other hand the glow curve temperature maximum (noted T_{max}) as a function of the excitation energy (left scale). For all excitations below 400 nm (above 3.1 eV), the peak maximum is observed around 318 K, whereas excitations above 400 nm lead to a maximum shifted around 333 K. Applying a thermal cleaning procedure to this main peak showed that the latter was not a single peak but was made of a continuous distribution of peaks (see the Supporting Information). Therefore, the shift in peak maximum observed is explained by the presence of several traps at slightly varying trap depths, more or less involved depending on the excitation energy. Below 400 nm excitation (above 3.1 eV), the shallowest traps of the distribution are

dx.doi.org/10.1021/cm403050q | Chem. Mater. 2014, 26, 1365−1373

filled, which shifts the peak to lower temperature, while excitation above 3.1 eV leads to the filling of the deepest traps and shifts the peak to higher temperature. This excitation-dependent variation of trap depths agrees well with the distribution of trap depth energies E_{dt} measured by thermal cleaning.

Therefore, we observe two distinct behaviors upon increasing the excitation wavelength. The low-temperature TSL peaks on the one hand show an intensity that decreases with lower excitation energy, while the main broad TSL peak on the other hand exhibits a shift of the temperature maximum toward high temperature. These two behaviors show a monotonous trend but also an abrupt change across the border value of ∼3.1 eV (see inset of Figure 6). This indicates again a change of regime in the TSL process at the photon energy threshold of 3.1 eV.

All these results indicate that the LLP mechanism is localized around Cr^{3+} ions for low photon energy excitation (down to 680 nm), corresponding mainly to the $^4A_2 \rightarrow {}^4T_2$ transition (range 1 in Figure 3). We may then consider that shorter wavelength (higher energy) excitation allows a charge separation over longer distance and/or at longer distances from Cr^{3+} centers. This is illustrated in Figure 4 by the presence of trapping levels at various distances from Cr^{3+} centers (red levels) that can be filled after excitation in any of the Cr^{3+} excited states. The farthest traps being the shallowest, the TSL peak tends to shift to lower temperature when shorter excitation wavelength is used.

The shallow traps corresponding to low-temperature TSL peaks (145 and 200 K) present a different behavior. They are easily filled with excitation above 3.1 eV but very less efficiently filled for excitation below 3.1 eV. Further, those peaks show as intense Cr_R emission as Cr_{N2}, which means that all Cr^{3+} ions are involved in this case (Figure 5). As these shallow traps are filled through band-assisted excitation, they may be located below the bottom of the CB and above the top of the VB, and at long distances from Cr^{3+} ions. These shallow electron−hole traps are represented as a blue level in Figure 4. This model agrees with the results of Figure 7 that show TSL glow curves

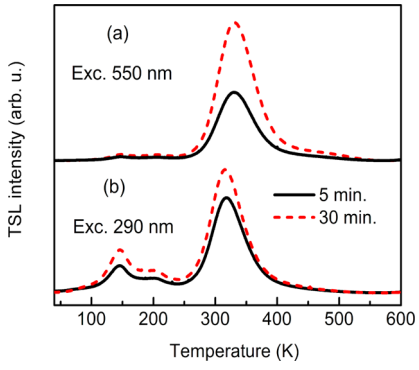

Figure 7. TSL glow curves of ZGO:Cr with varying excitation times at 10 K with (a) 550 and (b) 290 nm laser excitation.

recorded for various excitation times at two different wavelengths below and above 400 nm (3.1 eV). By increasing the 550 nm excitation time (in the $^4T_2$ state) from 5 to 30 min, the main TSL peak intensity doubles, while the low-temperature peaks remain very weak. With increasing excitation time at 290 nm, both low-temperature and main peaks increase by the same amount. Prolonged 550 nm excitation is therefore very inefficient to reach and fill the shallow traps (blue level in Figure 4). On the contrary, prolonging 290 nm excitation increases the probability of both deep trapping in the vicinity of Cr^{3+} centers and shallow trapping farther away. However the fact that TSL peaks at low temperatures are observed, even though with a very weak intensity, for excitation below 3.1 eV (mainly in the $^4T_2$ state, see Figure 6) show that these shallow traps can still be reached with weak efficiency. This is therefore explained by a second excitation from the filled deep traps (red levels in Figure 4), as represented by the interrupted black arrow.

Let us now consider again the results shown by spectra in Figure 5b, where Cr_R ions showed most intense emission in low-temperature TSL peaks (shallow trapping far from Cr^{3+} ions), whereas Cr_{N2} ions showed most intense emission in high-temperature TSL peak (deeper traps close to Cr^{3+} ions). This is fully consistent with the definition of Cr_{N2} and Cr_R ions, as Cr_{N2} ions occupy sites distorted by an antisite defect as first cationic neighbor, and possibly with more defects clustered around, whereas Cr_R ions do not have any distortion in their first cationic sphere.

The last point to be addressed is the nature of the carriers produced by excitation of Cr^{3+} ions (electrons, holes, or both). Although the LLP mechanism would be classically interpreted as an electron escaping from Cr^{3+} to a positively charged defect, we have strong experimental evidence against any change in the charge state of Cr^{3+} in ZGO:Cr between storage and emission steps. Transmission spectra of ZGO:Cr shown in Figure 8a

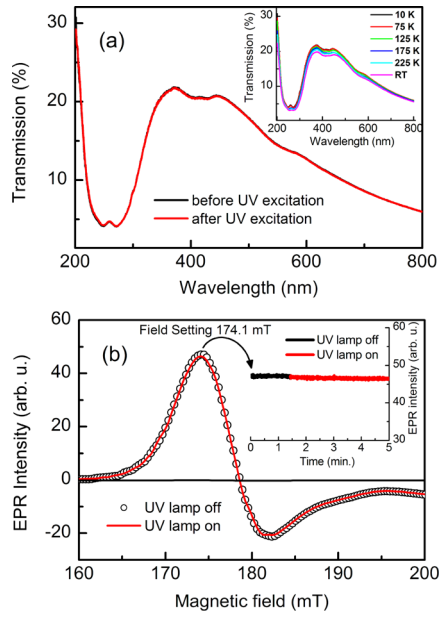

Figure 8. (a) Effect of a 30 min long UV irradiation on the optical transmission spectrum of ZGO:Cr at 10 K. Insert: transmission spectra at various temperatures after the prolonged UV irradiation. (b) Effect of a prolonged UV irradiation on the EPR spectrum of ZGO:Cr at 10K. Insert: EPR intensity at 174.1 mT in the dark and during UV illumination.

display the expected d−d absorption bands of Cr^{3+} at 555, 420, and 260 nm as well as the band gap transition at 255 nm. The main graph shows that the spectrum at 10K remains exactly identical before and after a 30 min long intense UV illumination although such a strong illumination provokes an intense LLP in ZGO:Cr.[16] Further no drastic change occurred when temperature was raised up to RT (see inset of Figure 8a).

dx.doi.org/10.1021/cm403050q | Chem. Mater. 2014, 26, 1365−1373

A conversion of Cr^{3+} into Cr^{4+} (or Cr^{2+}) during UV illumination would have induced a decrease in Cr^{3+} absorption bands as well as the appearance of Cr^{4+} (or Cr^{2+}) signature. Therefore, no evidence of electron or hole release from Cr^{3+} was shown here. This result is further confirmed by EPR. Figure 8b shows the low magnetic field component of ZGO:Cr EPR spectrum recorded at 10 K. The black baseline corresponds to the EPR spectrum of undoped ZGO while black open circles represent the spectrum of Cr^{3+} in the doped compound. As will be described in more detail in a separate paper, this EPR line corresponds to a transition between effective $M_s = \pm 1/2$ states in the $^4A_2$ ground state of Cr^{3+} ions with C_3 crystal field axis perpendicular to the magnetic field. By in situ irradiating the sample with UV (inside the EPR cavity) we observed that the EPR spectrum under UV (red line) is perfectly superimposed to the one in the dark (black open circles). This indicates that all chromium ions remain in the Cr^{3+} state during irradiation. This is confirmed by monitoring the EPR intensity at 174.1 mT (maximum of the EPR amplitude) in the dark and then during UV illumination (black and red traces in the insert of Figure 8b). As this field setting corresponds to the sensitivity maximum, the fact that the EPR intensity is constant indicates that chromium remains in the Cr^{3+} state during UV irradiation, in agreement with optical absorption experiment. We therefore conclude that the carriers released during excitation in the LLP/TSL process are electron−hole pairs instead of individual electrons or holes.

LLP MECHANISM

LLP has a long story starting with the famous Bologna stone in the beginning of the 17th century.[32,33] However all proposed mechanisms for LLP remained largely speculative prior to the discovery of the bright LLP of Eu^{3+}−R^{3+} codoped aluminate materials (R^{3+} = rare earth).[34,35] Important progress in understanding mechanisms was made possible by locating the energy levels of dopants and codopants with respect to host bands.[36] Based on this, a mechanism was proposed whereby Eu^{2+} is excited and liberates an electron in the conduction band (giving Eu^{3+}) and then trapped at R^{3+} site. This model allowed the design and control of persistent luminescence in several materials by predicting the energy levels of a system (band gap, luminescent center, codopant).[19,37,38] However, despite interesting predictive character brought by this model, experimental evidence often shows that mechanisms are more complex than expected and depend on the material considered. For example, X-ray absorption spectroscopy of Eu^{2+}-Dy^{3+} aluminate showed no evidence of direct electron trapping by R^{3+} ion, and the electron release from Eu^{2+} seems to involve only a limited fraction of Eu^{2+} ions.[39] Here, experimental results on ZGO:Cr showed that LLP induced by direct excitation of Cr^{3+} involves no change of its valence state, i.e., the metal ion does not liberate an electron (leading to Cr^{4+}) or a hole (leading to Cr^{2+}). Moreover the fact that LLP can be excited by orange-red light questions the usually compulsory participation of host bands to LLP. The present work shows several indications that the LLP mechanism in ZGO:Cr involves release and trapping of neutral electron−hole pairs and that this mechanism is localized in the vicinity of Cr_{N2} ions.

We propose in the following a mechanism based on the existence of a cationic disorder in spinels[14,15] as described by reaction 1 using the Kröger−Vink notation:

$$Zn_{Zn}^{\times} + Ga_{Ga}^{\times} \rightarrow Zn_{Ga}^{\prime} + Ga_{Zn}^{\circ} \quad (1)$$

where Zn_{Zn}^{x} indicates a Zn ion in its site, and $Zn_{Ga}^{\prime}$ a Zn ion in a gallium site (antisite defect). Neutral, positive, and negative charges are represented by cross, dot, and dash superscripts, respectively. When one of the two possible antisite defects is in first cationic position to Cr^{3+}, a Cr_{N2} ion responsible for the N2 emission dominating LLP is formed while the opposite charge defect can lie at various distances away. Such a defect cluster is schematized in Figure 9.

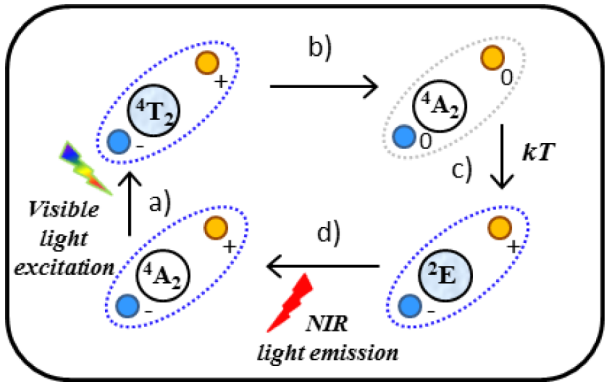

Figure 9. Proposed mechanism of LLP in ZGO:Cr induced by excitation below 3.1 eV. Cr_{N2} is represented by its states ($^4T_2$, $^4A_2$, or ^2E). Blue and yellow spheres represent the two opposite charge antisite defects. Steps: (a) optical excitation; (b) charge separation and carriers trapping by neighboring antisite defects of opposite charges; (c) thermal release of e^-—h^+ pairs and trapping by Cr^{3+}; (d) emission.

Let us first consider the mechanism occurring with excitation at energy lower than 3.1 eV. The basic idea is that each pair of opposite charge defects creates a local electric field at Cr^{3+}, which provides the driving force for charge separation. If we consider the $^4A_2$−$^4T_2$ chromium excitation, this corresponds to monoelectronic $(t_{2g})^3$−$(t_{2g})^2(e_g)^1$ transition. This means that in the excited state, an electron lies in the e_g orbital and a hole in t_{2g} orbitals. The $^4T_2$ state thus corresponds to a pair of an electron in e_g and a hole in t_{2g}. Each pair of antisite defects close to a Cr^{3+} ion (Cr_{N2}) acts as a trap for this electron−hole pair according to the reaction 2

$$(e^-—h^+) + Zn_{Ga}^{\prime} + Ga_{Zn}^{\circ} \rightarrow Zn_{Ga}^{\times} + Ga_{Zn}^{\times} \quad (2)$$

The mechanism is illustrated in Figures 4 and 9. The first step is the excitation of Cr_{N2}, for instance in the $^4T_2$ state by optical illumination at 550 nm (step a in Figure 9 and eq 3 below). The excitation, initially localized at Cr_{N2}, is then dissociated by the local electric field into an electron and a hole that get trapped at Ga_{Zn}° and $Zn_{Ga}^{\prime}$ neighboring defects, respectively, according to reaction 2 (path 1 in Figure 4 and step b in Figure 9). The excitation is trapped in the vicinity of chromium in the form of a pair of neutral defects Ga_{Zn}^{x} and Zn_{Ga}^{x} while Cr^{3+} returns to its $^4A_2$ ground state (step b in figure 9 and eq 4 below). The electron (hole) trapping by Ga_{Zn}° ($Zn_{Ga}^{\prime}$) is thus strictly equivalent to an optically induced donor−acceptor (D−A) transfer from Zn_{Ga} (D) to Ga_{Zn} (A). As the spin state $S = 3/2$ of Cr_{N2} is conserved during irradiation and trapping, the total spin of the Ga_{Zn}^{x}−Zn_{Ga}^{x} pair is $S = 0$, corresponding to spin paired electron−hole pair. By considering an elementary Cr_{N2} ion as a defect cluster written $[Cr^{3+}(^4A_2),Ga_{Zn}^{\circ}\text{-}Zn_{Ga}^{\prime}]_{N2}$, the mechanism for persistent luminescence can be represented by reactions 3 to 5, for instance in the case of a $^4A_2 \rightarrow {}^4T_2$ initial excitation

dx.doi.org/10.1021/cm403050q | Chem. Mater. 2014, 26, 1365−1373

$$[Cr^{3+}(^4A_2),\ Ga^{\circ}_{Zn}—Zn'_{Ga}]_{N2} \xrightarrow{h\nu} [Cr^{3+}(^4T_2),\ Ga^{\circ}_{Zn}—Zn'_{Ga}]_{N2} \quad (3)$$

$$[Cr^{3+}(^4T_2),\ Ga^{\circ}_{Zn}—Zn'_{Ga}]_{N2} \rightarrow [Cr^{3+}(^4A_2),\ Ga^{\times}_{Zn}—Zn^{\times}_{Ga}]_{N2} \quad (4)$$

It is important to note that the local electric field responsible for charge separation in the excited state of Cr_{N2} vanishes after reaction 4, as antisite defects become neutral after electron−hole trapping. The reverse reaction (electron−hole release and capture by Cr^{3+}) is thermally activated, with the activation energy E_{dt} (deep trap) responsible for the main TSL peak around 318 K, according to the following reaction (steps c and d in Figure 9 and eq 5 below):

$$[Cr^{3+}(^4A_2),\ Ga^{\times}_{Zn}—Zn^{\times}_{Ga}]_{N2} \xrightarrow{kT} [Cr^{3+}(^4T_2),\ Ga^{\circ}_{Zn}—Zn'_{Ga}]_{N2} \rightarrow [Cr^{3+}(^2E),\ Ga^{\circ}_{Zn}—Zn'_{Ga}]_{N2} \rightarrow [Cr^{3+}(^4A_2),\ Ga^{\circ}_{Zn}—Zn'_{Ga}]_{N2} + h\nu \quad (5)$$

The observed distribution of temperature in TSL is due to a distribution of energies for the deep traps along the configuration coordinate (red curves in Figure 4), corresponding to a distribution of distances (and therefore of electric fields) between the two complementary antisite defects around Cr_{N2}.

By exciting above 3.1 eV, the Cr^{3+} excited states are degenerated with free e^-—h^+ states (see Figure 4). This ensures an easier charge separation (path 2 in Figure 4), and the possibility for carriers to migrate over longer distances from the metal ion and to fill in shallow traps responsible for low-temperature TSL peaks (80, 145, and 205 K) with activation energy E_{ST} (blue level in Figure 4). This shallow trapping corresponds to reaction 2 and path 2 in Figure 4 (red dotted arrows). In this high photon energy regime, the fact that host bands are involved implies that the mechanism is then not necessarily localized around Cr^{3+}. This explains why both Cr_R and Cr_{N2} contribute to the low-temperature TSL peaks.

■ CONCLUSION

$ZnGa_2O_4$:Cr^{3+} spinel materials were recently shown to present exceptional persistent luminescence properties. They were reported as very efficient LLP compounds[15,16,20] and particularly attracted attention by the possibility to activate their LLP by using a wide range of UV−visible excitation. This gave rise to exciting applications like sunlight-activated taggants in night-vision surveillance[20] or red-activated probes for small animal bioimaging,[17] with an emission properly located in the near-infrared part of the spectrum. In the present paper, we investigated the mechanism of this LLP, activated by virtually all wavelengths of the visible range. We took advantage of Cr^{3+} that constitutes, by substituting Ga^{3+} in the spinel structure, a very fine optical and paramagnetic probe of its local environment. We could therefore demonstrate that LLP occurred via the excitation of a specific type of Cr^{3+} ions, namely Cr_{N2}, having an antisite defect as first cationic neighbor. Exciting ZGO:Cr in any of the absorption bands of Cr_{N2} all over the visible range (down to 1.82 eV, 680 nm) therefore triggers LLP. An efficiency amplification by band assistance, however, was clearly shown to exist above the threshold value of 3.1 eV (400 nm) because of the position of Cr^{3+} states relative to free e^-—h^+ states. However, the same TSL peak at 318 K, responsible for LLP at RT, was observed for both above and below 3.1 eV excitation. LLP can therefore take place at low photon energy without any participation of the host bands following a mechanism entirely localized around Cr_{N2}. The essential features of the proposed mechanism are the following: (i) the excitation and trapping steps of LLP involve pairs of antisite defects, one antisite defect being adjacent to a Cr^{3+} ion (forming a Cr_{N2} ion); (ii) these two steps involve excitation and trapping of an electron−hole pair; (iii) after excitation, Cr^{3+} (Cr_{N2}) ion returns to its $^4A_2$ ground state while the excitation being trapped by a neighboring pair of antisite defects; (iv) in the model, the driving force for charge separation in the excited state of chromium is the local electric field created by the pair of neighboring antisite defects; (v) a distribution of distances between the opposite charge defects exist and can be reached depending on the excitation wavelength used. This localized mechanism involving only Cr_{N2} in the excitation, trapping and emission steps of LLP implies that Cr_{N2} ions are able to store visible light in ZGO:Cr. The TSL study extended to low temperature complemented the investigation and explained processes of trapping by shallower traps. These processes were shown to occur at farther distances from Cr^{3+} ions and therefore concerned all types of Cr^{3+} ions including defect-free Cr_R ions. Optimization of $ZnGa_2O_4$:Cr^{3+} compounds for biomedical application is currently under work.

■ ASSOCIATED CONTENT

Ⓢ Supporting Information

TSL of ZGO:Cr was analyzed by two methods: thermal cleaning (Figure S1) and variation of the sample temperature during excitation (Figure S2). This material is free of charge via the Internet at http://pubs.acs.org.

■ AUTHOR INFORMATION

Corresponding Authors

*E-mail: aurelie.bessiere@chimie-paristech.fr.
*E-mail: didier.gourier@chimie-paristech.fr.

Notes

The authors declare no competing financial interest.

■ ACKNOWLEDGMENTS

Authors acknowledge the Indo-French Centre for the Promotion of Advanced Research (IFCPAR)/ Centre Franco-Indien Pour la Recherche Avancée (CEFIPRA) for financial support.

■ REFERENCES

(1) Yen, W. M.; Shionoya, S.; Yamamoto, H. *Practical Applications of Phosphors*; CRC Press: Boca Raton, FL, 2006.
(2) le Masne de Chermont, Q.; Chanéac, C.; Seguin, J.; Pellé, F.; Maîtrejean, S.; Jolivet, J.-P.; Gourier, D.; Bessodes, M.; Scherman, D. *Proc. Nalt. Acad. Sci. U.S.A* **2007**, *104* (22), 9266−71.
(3) le Masne de Chermont, Q.; Scherman, D.; Bessodes, M.; Pellé, F.; Maitrejean, S.; Jolivet, J.-P.; Chanéac, C.; Gourier, D. Nanoparticules à luminescence persistante pour leur utilisation en tant qu'agent de diagnostique destiné à l'imagerie optique in vivo, CNRS patent, internat ext. WOEP06067950, WO2007048856, 30/10/2006.
(4) Maldiney, T.; Byk, G.; Wattier, N.; Seguin, J.; Khandadash, R.; Bessodes, M.; Richard, C.; Scherman, D. *Int. J. Pharm.* **2012**, *423*, 102−107.

(5) Maldiney, T.; Kaikkonen, M. U.; Seguin, J.; le Masne De Chermont, Q.; Bessodes, M.; Airenne, K. J.; Ylä-Herttüala, S.; Scherman, D.; Richard, C. *Bioconjugate Chem.* **2012**, *23*, 472−478.
(6) McKeever, S. W. S. *Thermoluminescence of Solids*; Cambridge Solid State Science Series; Cambridge University Press: Cambridge, U.K., 1988.
(7) Hoogenstraaten, W.; Klasens, H. A. *J. Electrochem. Soc.* **1953**, *100*, 336.
(8) Matsuzawa, T.; Aoki, Y.; Takeuchi, N.; Maruyama, Y. *J. Electrochem. Soc.* **1996**, *143*, 2670.
(9) Aitasalo, T.; Deren, P.; Holsa, J.; Jungner, H.; Krupa, J.; Lastusaari, M.; Legendziewicz, J.; Niittykoski, J.; Strek, W. *J. Solid State Chem.* **2003**, *171*, 114.
(10) Van den Eeckhout, K.; Smet, F. S.; Poelman, D. *Materials* **2010**, *3*, 2536−2566.
(11) Maldiney, T.; Lecointre, A.; Viana, B.; Bessière, A.; Bessodes, M.; Gourier, D.; Richard, C.; Scherman, D. *J. Am. Chem. Soc.* **2011**, *133*, 11810−11815.
(12) Lecointre, A.; Bessière, A.; Priolkar, K. R.; Gourier, D.; Wallez, G.; Viana, B. *Mater. Res. Bull.* **2013**, *48*, 1898−1905.
(13) Brito, H. F.; Hölsä, J.; Laamanen, T.; Lastusaari, M.; Malkamäki, M.; Rodrigues, L. C. V. *Optic. Mater. Express* **2012**, *2*, 371−381.
(14) Errandonea, D.; Kumar, R.; Manjón, F.; Ursaki, V.; Rusu, E. *Phys. Rev. B* **2009**, *79*, 024103.
(15) Allix, M.; Chenu, S.; Ve, E.; Poumeyrol, T.; Kouadri-boudjelthia, E. A.; Alahrache, S.; Porcher, F.; Massiot, D. *Chem. Mater.* **2013**, *25*, 1600−1606.
(16) Bessière, A.; Jacquart, S.; Priolkar, K.; Lecointre, A.; Viana, B.; Gourier, D. *Opt. Express* **2011**, *19*, 10131−10137.
(17) Maldiney, T.; Richard, C.; Scherman, D.; Gourier, D.; Viana, B.; Bessière, A. "Nanoparticules à luminescence persistante excitable in situ pour l'imagerie optique in vivo, l'imagerie multimodale optique-IRM in vivo et la théranostique". Patent PCT/EP2013/051727, 30/01/2013.
(18) Bessière, A.; Lecointre, A.; Benhamou, R. A.; Suard, E.; Wallez, G.; Viana, B. *J. Mater. Chem. C* **2013**, *1*, 1252−1259.
(19) Lecointre, A.; Bessière, A.; Bos, A. J. J.; Dorenbos, P.; Viana, B.; Jacquart, S. *J. Phys. Chem. C* **2011**, 4217−4227.
(20) Pan, Z.; Lu, Y.-Y.; Liu, F. *Nat. Mater.* **2011**, *11*, 58−63.
(21) Zhuang, Y.; Ueda, J.; Tanabe, S. *App. Phys. Express* **2013**, *6*, 052602.
(22) Bos, A. J. J.; van Duijvenvoorde, R. M.; van der Kolk, E.; Drozdowski, W.; Dorenbos, P. *J. Lumin.* **2011**, *131*, 1465−1471.
(23) Kahan, H. M.; Macfarlane, R. M. *J. Chem. Phys.* **1971**, *54*, 5197−5205.
(24) Derkosh, J.; Mikenda, W. *J. Lumin.* **1983**, *28*, 431−441.
(25) Nie, W.; Michel-Calendini, F. M.; Linares, C.; Boulon, G.; Daul, C. *J. Lumin.* **1990**, *46*, 177−190.
(26) Zhang, W.; Zhang, J.; Chen, Z.; Wang, T.; Zheng, S. *J. Lumin.* **2010**, *130*, 1738−1743.
(27) Mikenda, W. *J. Lumin.* **1981**, *26*, 85−98.
(28) Karazhanov, S. Z.; Ravindran, P. *J. Am. Ceram. Soc.* **2010**, *93*, 3335−3341.
(29) Sampath, S. K.; Cordaro, J. F. *J. Am. Ceram. Soc.* **1998**, *81*, 649−654.
(30) Tanabe, Y.; Sugano, S. *J. Phys. Soc. Jpn.* **1954**, *9*, 766−779.
(31) Randall, J. T.; Wilkins, M. H. F. *Proc. R. Soc. London, Ser. A* **1945**, *184*, 366−389.
(32) Licetus, F. *Litheosphorus Sive de Lapide Bononiensi*; Universitàdi Bologna: Bologna, Italy, 1640.
(33) Lastusaari, M.; Laamanen, T.; Malkamaki, M.; Eskola, K. O.; Kotlov, A.; Carlson, S.; Welter, E.; Brito, H. F.; Bettinelli, M.; Jungner, H.; Holsa, J. *Eur. J. Miner.* **2012**, *24*, 885−890.
(34) Yamamoto, H.; Matsuzawa, T. *J. Lumin.* **1997**, *72*−*74*, 287−289.
(35) Matsuzawa, T.; Aoki, Y.; Takeuchi, N.; Murayama, Y. *J. Electrochem. Soc.* **1996**, *143*, 2670−2673.
(36) Dorenbos, P. *J. Lumin.* **2004**, *108*, 301−305.
(37) Rodrigues, L. C. V.; Brito, H. F.; Hölsä, J.; Lastusaari, M. *Opt. Mater. Express* **2012**, *2*, 382−391.
(38) Jia, D.; Wang, J.; Yen, W. M. *Chem. Phys. Lett.* **2002**, *363*, 241−244.
(39) Korthout, K.; Van den Eeckhout, K.; Botterman, J.; Nikitenko, S.; Poelman, D.; Smet, P. *Phys. Rev. B* **2011**, *84*, 085140.